Detection of magnetite in the Roossenekal area of the Eastern Bushveld Complex, South Africa, using multispectral remote sensing data

M. Twala
Department of Geology, University of Pretoria, Lynnwood road, Pretoria, South Africa, 0002
e-mail: mthokozisi.thwala@gmail.com

R. J. Roberts
Department of Geology, University of Pretoria, Lynnwood road, Pretoria, South Africa, 0002
e-mail: james.roberts@up.ac.za

C. Munghemezulu
Department of Geography, Geoinformatics and Meteorology, University of Pretoria, South Africa
Agricultural Research Council-Institute for Soil, Climate and Water (ARC-ISCW), Division of Geoinformation Science, Pretoria, South Africa
e-mail: cilence.munghemezulu@up.ac.za

Abstract

Multispectral sensors, along with common and advanced algorithms, have become efficient tools for routine lithological discrimination and mineral potential mapping. It is with this paradigm in mind that this paper sought to evaluate and discuss the detection and mapping of magnetite on the Eastern Limb of the Bushveld Complex, using high spectral resolution multispectral remote sensing imagery and GIS techniques. Despite the wide distribution of magnetite, its economic importance, and its potential as an indicator of many important geological processes, not many studies had looked at the detection and exploration of magnetite using remote sensing in this region. The Maximum Likelihood and Support Vector Machine classification algorithms were assessed for their respective ability to detect and map magnetite using the PlanetScope Analytic data. A K-fold cross-validation analysis was used to measure the performance of the training as well as the test data. For each classification algorithm, a thematic landcover map was created and an error matrix, depicting the user's and producer's accuracies as well as kappa statistics, was derived. A pairwise comparison test of the image classification algorithms was conducted to determine whether the two classification algorithms were significantly different from each other. The Maximum Likelihood Classifier significantly outperformed the Support Vector Machine algorithm, achieving an overall classification accuracy of 84.58% and an overall kappa value of 0.79. Magnetite was accurately discriminated from the other thematic landcover classes with a user's accuracy of 76.41% and a producer's accuracy of 88.66%. The overall results of this study illustrated that remote sensing techniques are effective instruments for geological mapping and mineral investigation, especially iron oxide mineralization in the Eastern Limb of the Bushveld Complex.

Introduction

Remote sensing is the acquisition of information and the identification of Earth-surface features or phenomena using reflected and emitted electromagnetic radiation (from the surface-features), measured by sensors on airborne or

spaceborne platforms (Drury, 2001; Agar and Coulter, 2007; Ngcofe and Van Niekerk, 2016; Joseph and Bamidele, 2018). Remote sensing provides quantitative observational parameters for large areas and hence, is an essential source of information for many geological investigations (Abrams et al., 1983; Clark and Roush, 1984; Chung and Rencz, 1994; Agar and Coulter, 2007; Rajendran et al., 2007; Li et al., 2016; Manuel et al., 2017; Joseph and Bamidele, 2018; Izawa et al., 2019). In the last century, remote sensing has been extensively used in many geological applications. Most notably in geological mapping, mineral exploration, and geotechnical investigations, where it saves both time and initial investments, by giving a synoptic view of the sites of interest, which are often difficult to obtain from field-based observation alone (Ngcofe and Van Niekerk, 2016; Manuel et al., 2017).

The advantages and disadvantages of remote sensing in mineral exploration have been extensively studied (Cloutis, 1996; Agar and Coulter, 2007; Gupta, 2017). For similar reasons which impede field geology, the application of remote sensing for mapping geological features is fraught with both practical as well as conceptual difficulties such as: inadequate sensor spatial resolutions, the reliance on exposed lithologies for direct sensing or outcrops, and the erroneous detection of spectrally composite spectral signatures as a result of the mixing of pure end-member signatures of vegetation, soil, and regolith (Metternicht and Zinck, 2003; Kemp et al., 2005; Wang and Qu, 2009; Campbell and Wynne, 2011). Indeed, it is worth noting that satellite remote sensing is not a replacement for direct fieldwork and laboratory studies; on the contrary, the best analysis of the results is reliably acquired from the amalgamation of different data and even from analysis at different scales and perspectives. Despite satellite remote sensing not being a replacement for direct fieldwork and more traditional methods, remote sensing can provide additional and crucial information for preliminary geological investigations (Kemp et al., 2005). Although remote sensing tools have been regularly utilized for diverse aspects of geosciences in South Africa, with the notable exception of a handful of publications, there is a lack of studies regarding its specific use in iron oxide exploration, especially in the Bushveld Complex.

The significant progress made in multispectral remote sensing, has led to a vast variety of supervised and unsupervised classification algorithms evolving, with each algorithm used with the intent of accurately and efficiently detecting and classifying lithological features (Schetselaar et al., 2000; Inzana et al., 2003; Rowan and Mars, 2003; Kemp et al., 2005; Rowan et al., 2005; Fatima et al., 2013; Babakan and Oskouei, 2014; Shirazi et al., 2018). Supervised classification, which entails the assigning of samples of identical pixels to classes that exhibit the same tonality, texture, and shape to each class has been met with tremendous success in geological mapping. The image classification algorithm Maximum Likelihood has wide-ranging popularity in its application in remote sensing image classification (Jensen, 2005). The classification algorithm is based on a parametric approach that assumes a normal Gaussian distribution of the selected classes (Kavzoglu and Reis, 2008; Mondal et al., 2012).

Decision Trees, Fuzzy C-Mean, Support Vector Machines, and Artificial Neural Networks are just some of the few well-known non-parametric classification algorithms. The predominately used non-parametric algorithm is the Support Vector Machine classification algorithm. Support Vector Machines are a group of supervised classification algorithms that compare favourably with more established common remote sensing algorithms. Support Vector Machines are considered to be heuristic algorithms based on statistical theory, which is used for classification and regression problems (Vapnik, 1999; Vapnik, 2013). The classification accuracy of Support Vector Machines may vary depending on the choice of the kernel function and its parameters (Kavzoglu and Colkesen, 2009; Yu et al., 2012).

To further increase the landcover discrimination ability of classification algorithms, various high-resolution satellite sensors have been launched, with some having the capability of generating remote sensing imagery with a spatial resolution of 4 m or less in multispectral mode. Table 1, briefly lists some characteristics of known satellites and sensors predominately used for lithological mapping and mineral detection.

Spatial resolution specifies the dimensions of the satellite image pixels, i.e. the higher or finer the spatial resolution, the more detail the sensor is able to provide for the ground cover. The spatial resolution is contingent on the desired object of observation. The spectral resolution determines the number of spectral bands reflected radiance that can be collected by the sensor or the range of wavelengths a single band covers.

Table 1. Characteristics of satellite and sensors frequently used for lithological mapping and mineral detection.

Satellite	Sensor	Launch	Spectral resolution	Spatial resolution (m)	Country of ownership
LANDSAT	TM, MSS	1976	7 visible and 1 thermal IR band; 0.50- 12.5 µm spectral resolution	30 - 80	USA
SPOT	HRV	1986	3 visible and 1 IR band; 0.50- 0.73 µm spectral resolution	10 - 20	France
RapidEye	Jena-Optronik	2008	4 visible and 1 IR band; 0.44- 0.88 µm spectral resolution	5	USA
LANDSAT-7	ETM	1999	8 visible and 1 thermal IR band; 0.45- 12.5 µm spectral resolution	15 - 60	USA
LANDSAT-8	OLI, TIRS	2013	9 visible, 1 and thermal IR band; 0.433- 12.50 µm spectral resolution	15, 30, 100	USA
SPOT-5	HRS, HRG	2002	4 visible and 1 IR band; 0.50- 0.71 µm spectral resolution	10, 20	France
TERRA (EOS AM-1)	ASTER	1999	14 visible and 5 IR bands; 0.53- 11.65 µm spectral resolution	15 - 90	USA

The more bands a sensor has, the better equipped it is to identify and characterise natural materials (Congalton, 2001; Gupta, 2017).

Radiometric resolution refers how fine a sensor divides up the radiance it receives in each band and therefore is an indicator of the amount of information is in contained in each pixel. The finer the radiometric resolution the greater the sensitivity of radiation the sensor is able to detect (Gupta, 2017). However, owing to the difficulty and exorbitant costs of obtaining imagery with an extremely high resolution, it is often necessary to identify resolutions which are paramount for a project, in a process known as "trade-offs". Either the spatial resolution is high, but the spectral and radiometric resolution are low or vice versa. Since the dimensions of the smallest magnetite bodies recorded for this study were approximately 3 m (7.07 m^2), a sensor with spatial resolution of 3 m with a fine spectral and radiometric resolution to distinguish and detect the slightest changes in radiance from magnetite and other geological material was required. However, as conveyed in Table 1, it is not plausible to have a sensor with high spatial, spectral, and radiometric resolution.

However, for this study, offerings from an American based private company provided the some of the best trade-offs for the detection of magnetite relative to the sensor in Table 1. Planet Team (2018) offers three earth observation products: a Basic Scene product, an Ortho Scene product, and an Ortho Tile. Planet Team (2018) has a complete constellation of over 150 satellites imaging the entire surface of the earth every day with a spatial resolution of 3 m, a spectral resolution of four bands (blue, green, red and NIR), and a radiometric resolution of 16-bits, with a position accuracy of less than 10 m residual standard error (RSE) and a daily revisit capability.

This paper sought to evaluate and discuss the detection and mapping of magnetite on the Eastern Limb of the Bushveld Complex, with the aid of supervised classification algorithms, Maximum Likelihood and Support Vector Machines, based on awareness of previous successes and performance. Furthermore, this paper sought to contrast the overall efficiency of the different classification algorithms using PlanetScope imagery. The accuracy of each algorithm was assessed using the collected reference data. User's and producer's accuracy, and errors of commission and omission are used as comparative indices of measure of the efficiencies of each of the two supervised classification algorithms. The user's accuracy is an indicator of how well the training data was accurately distinguished. On the other hand, the producer's accuracy is an indicator of the model's ability to predict itself.

Geological setting

The Rustenburg Layered Suite, from henceforth referred to as the Eastern Limb of the Bushveld Complex, consists of a *ca.* 7 to 9 km thick basic and ultrabasic cumulate sequence outcropping in three limbs (Northern, Eastern, and Western Limb) (Eales and Cawthorn, 1996; Fischer et al., 2016). This thesis focuses on the Eastern Limb. In each limb, these cumulates are divided into: Marginal, Lower, Critical, Main, and Upper Zones (Figure 1, Von Gruenewaldt, 1971; SACS, 1980; Fischer et al., 2016).

The area northeast of Roossenekal, is one of the relatively few areas where rocks of the Upper Zone are well exposed (Von Gruenewaldt, 1971). It is comprised of a *ca.* 2 km thick stratigraphic layer, which hosts the largest vanadium deposit in the world (Willemse, 1969). Furthermore, the Upper Zone is renowned for the occurrence of numerous layers of magnetite and nelsonite (Tegner et al., 2006). Magnetite is a striking feature and a common constituent in virtually all the rock types found in the Upper Zone. It constitutes, on average, between 8 to 10 % by volume of the rocks (Grant, 2015).

Twenty-five magnetitite layers have been identified in the Eastern Limb, with a combined thickness of approximately 20.4 m (Tegner et al., 2006). The individual magnetitite layers range from 0.1 m to 10 m in thickness (Harne and Von Gruenewaldt, 1995). The lower three magnetitite layers (layers 1 to -3) are located below the Main Magnetitite Layer, and Magnetite Layers 4 to -21 are located above the Main Magnetitite Layer (Figure 2) (Maila, 2015). The magnetitite layers extend laterally approximately 100 km in the Eastern Limb of the Bushveld Complex, illustrating remarkable continuity (Cawthorn, 1994). In comparison to the upper contacts of the magnetitite layers, which undergo a gradational change to anorthosite, the lower contacts of the magnetitite layers and the host rocks and the underlying anorthosite are typically sharp (McCarthy et al., 1985; Reynolds, 1985). The gradational change from magnetitite to anorthosite on the upper contacts of the magnetitite layers could be a result of crystal sedimentation.

The Upper Zone has been divided into sub-zones, namely; A, B, and C. The base of the Upper Zone (sub-zone A) has been defined by the South African Committee for Stratigraphy (SACs) (SACS, 1980; Grant 2015) as being the level where magnetite makes its appearance in the succession. Magnetite-bearing leucogabbronorite, gabbronorite, gabbro and anorthosite dominate this sub-zone.

The base of sub-zone B is marked by the appearance of iron-rich olivine and magnetite bearing gabbro (Harne and Von Gruenewaldt, 1995). The appearance of cumulus apatite marks the base of sub-zone C, which is dominated by magnetite bearing gabbro and magnetite bearing olivine and diorite; however, olivine-free rocks are present in the vicinity of magnetitite layers (Von Gruenewaldt, 1976). Apatite appears cyclically in Upper Zone (C) has a sub-rounded texture, with grain sizes varying from *ca.* 0 to 2 mm embedded in Fe-Ti oxides. Throughout the Upper Zone, sulphides are few and far between but may occur with magnetitite layers (Von Gruenewaldt, 1976).

Data description and pre-processing

The PlanetScope Analytic Ortho Tiles used for the creation of the thematic map of the study site and for the detection of magnetite were sourced from Planet Explorer (Planet Team, 2018), for the date 03 December 2018, which had the highest image quality and the lowest land and scene cloud cover closest to the date of sampling. Furthermore, the choice of the PlanetScope Analytic Ortho Tiles was contingent on the

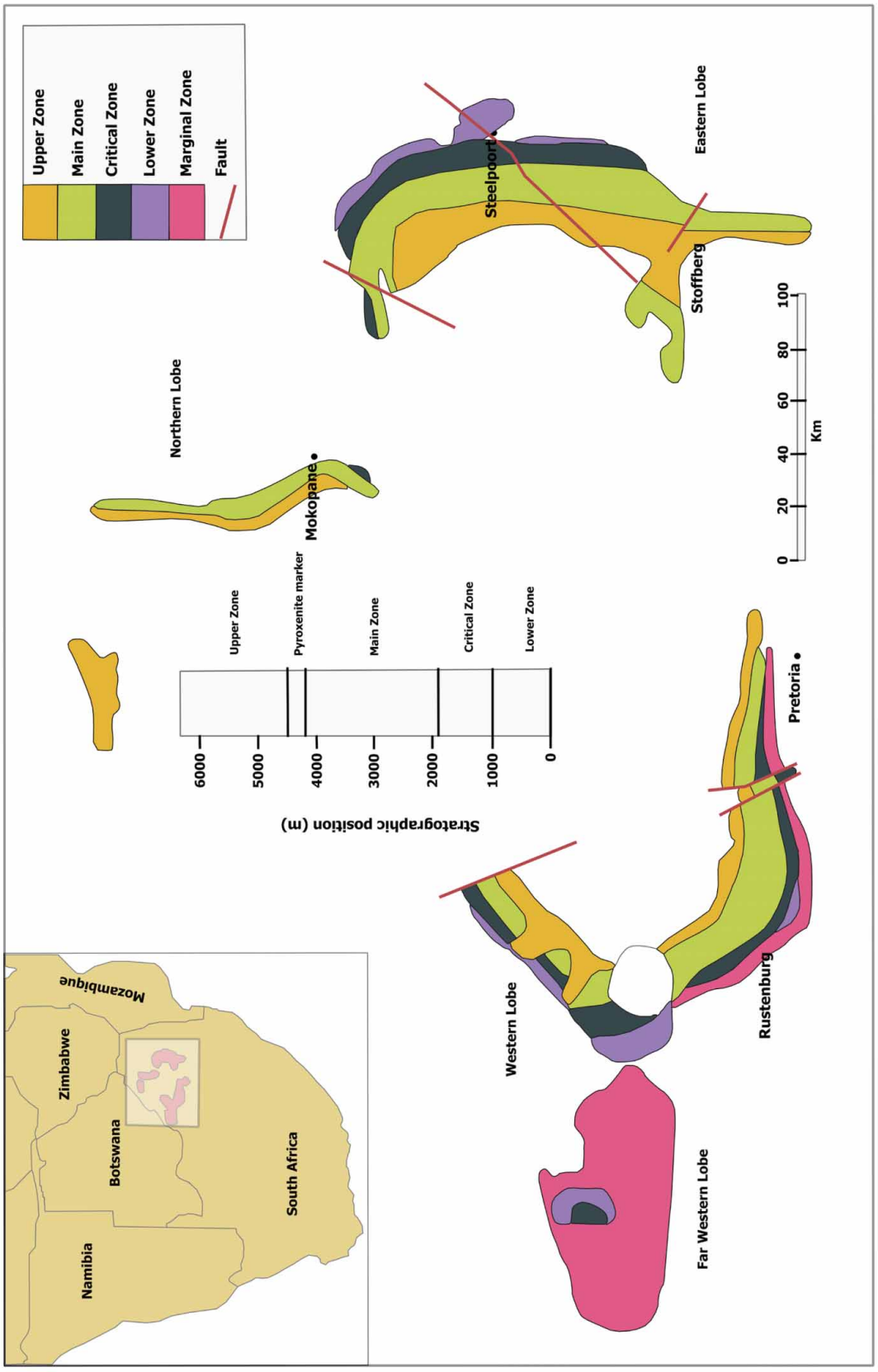

Figure 1. *Location of the various limbs of the Bushveld Complex, modified after Chistyakova et al. (2019).*

vegetation cover on the chosen magnetite sites (explained in the next section). The PlanetScope Analytic Ortho Tiles are corrected for geometric-, sensor-, and radiometric interferences and have been aligned to a cartographic map projection (UTM WGS 84). Image mosaicking was applied, using a pixel-based mosaicking function, for the ortho-tiles covering the area interest.

Field sampling

The regions of interest for the different classes of training and validation data used for this study were collected at known or previously visited localities on the 19 March 2019 to 23 March 2019. A variety of localities covering the different types of magnetite and landcover types were visited, those which were accessible by road and were well exposed (i.e. not covered by

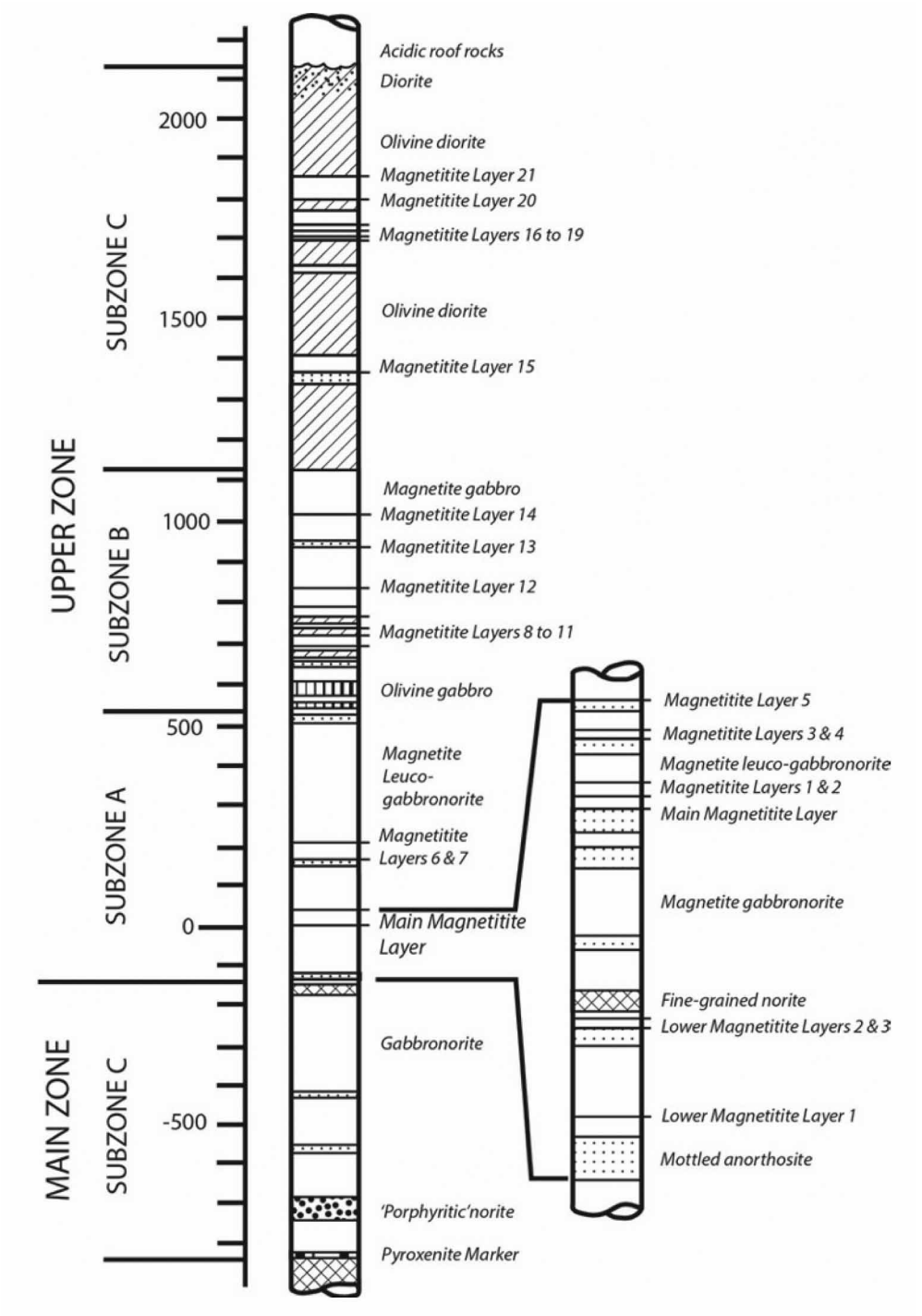

Figure 2. *Detailed stratigraphic sequence of the Upper Zone in the Eastern Limb of the Bushveld Complex (Harne and Von Gruenewaldt, 1995; Maila, 2015).*

vegetation and or soil- especially for magnetite) were chosen (Figure 3). Each region of interest for each class were sampled a minimum of 300 m apart, to avoid spatial autocorrelational. Although seasonal vegetation changes may have influenced some activities such as farming in the area, fieldwork was merely constrained by logistical and scheduling constraints.

Global Positioning System (GPS) coordinates covering the circumference of the region of interest were collected together with a brief description of the setting of the land-cover type and sample number. The GPS data collected was converted to ground reference areas or polygon delineations of the shape of each of the areas of interest, using QGIS 2.18 (QGIS Development Team, 2015). The ground reference data were used to train the algorithms used in ENVI (Exelis Visual Information Solutions, 2017) and python (Continuum Analytics, 2019). Accessibility to certain areas of interest and time were the main limitations in attaining a vast array of ground reference data. Hence, auxiliary GPS coordinate data were acquired from Google Earth (2018) images. The 120 areas of interest were combined into seven classes (Agricultural land, Grassland and trees, Residential areas, Waterbodies, Mining activities, regolith, and magnetite) and divided into training data and validation data. The pixel count from the regions of interest were log transformed in R 3.3.3 (R Core Team, 2016) (for the data to be normally distributed and to meet algorithm assumptions) and used in the Maximum Likelihood classification algorithms. Untransformed pixel count data was used for Support Vector Machines classification algorithm to catalogue the range of spectral data in the entire satellite image.

A *K-fold* cross-validation analysis (with the data divided into ten equal segments i.e. K = 10) was used to measure the performance of the training as well as the test data. The seed function, which randomizes the values, was set to 123. The K-value (K = 10) was chosen based on its ability to empirically yield test error rate estimates whose performance was not affected by excessively high bias and variance. The *K-fold* cross-validation analysis yields more accurate estimates of the test error rate than other cross-validation methods, such as Leave Out One Cross-validation (James et al., 2014). The analysis was performed in R 3.3.3 (R Core Team, 2016) using the basic packages 'car' (Fox and Weisberg, 2011), 'dplyr' (Wickham et al., 2015), 'tidyr' (Wickham and Henry, 2018), and 'readr' (Wickham et al., 2017). The analysis was evaluated using the R^2, Root Mean Squared Error (RSME), and Mean Absolute Error (MAE) statistics, which were outputs attained from the *K-fold* cross-validation analysis.

Description of classification algorithms

The Maximum Likelihood classification algorithm has been the most frequently used data-driven parametric classifier in remote sensing data classification (Foody et al., 1992; Jia et al., 2011). The Maximum Likelihood classification algorithm assumes that a hyper-ellipsoid decision volume can be utilized in approximating the shape of the data clusters. Moreover, for a given unidentified pixel, the likelihood of membership in each class is premeditated using the mean feature vectors of the classes, the covariance matrix and the prior probability (Chien, 1974). For normally distributed data, the Maximum Likelihood classification algorithm provides better predictive accuracy than the other parametric classifiers; however, for data that is not normally distributed the predictive accuracy may be unsatisfactory (ERDAS, 2005; Otukei and Blaschke, 2010).

The Support Vector Machine supervised classification algorithm is a data-driven technique that is based on statistical learning theory (Vapnik, 1999), and has been further developed in many other classification applications in the past decade. The algorithm aims to determine the location of decision boundaries that optimizes the greatest separation between the different classes (Pal and Mather, 2005; Vapnik, 1999; 2013). Considering the example of two classes which are linearly separated, the Support Vector Machine selects the linear decision boundary that minimizes the generalization error and leaves the greatest distance from the hyperplane or margin between the two classes (Vapnik, 1999; 2013). The data points closest to the hyperplane that are used to measure the distance from the hyperplane or margin are termed 'support vectors'. A Support Vector Machine tries to find the hyperplane that maximizes the margin, while minimizing the generalization error or the number of misclassifications (Pal and Mather, 2005). The choice of kernel function of Support Vector Machine classification algorithm (linear kernel, polynomial kernel, radial basis function kernel, and sigmoid kernel) is integral to its accuracy training and classifying remote sensing imagery. In this study, the radial basis function kernel was used because the remote sensing data was not linearly distributed.

Algorithm evaluation

The assessment of the accuracy and fitness of image classification algorithms has become a central component of studies that have sought to compare the abilities of the different algorithms in discriminating different classes (Congalton et al., 1983; Congalton, 2001; Congalton and Green, 2002; Mather and Koch, 2011; Mather and Tso, 2016). The aim of performing an accuracy assessment is to assess the fitness for use of the classified data. The classified map is compared to reference points where the classes of the landcover have already been determined. The accuracy of the classification is then calculated. Most often the error matrix technique is used as a method for assessing the accuracy and fitness of the thematic map for a particular purpose. Accuracy assessments determines the quality and accuracy of the information derived from remotely sensed data. The accuracy of the thematic map needs to be evaluated so that the user is made conscious of any potential problems that may be associated with the use of the thematic map. The end-product of the image classification process is a landcover or thematic map.

As previously introduced, an error matrix is a matrix that expresses the number of pixels or sample units that were correctly classified to a particular category in comparison to pixels or sample units belonging to another particular category being assigned to a different category or class (Congalton and Green, 2002). The columns represent the reference data or

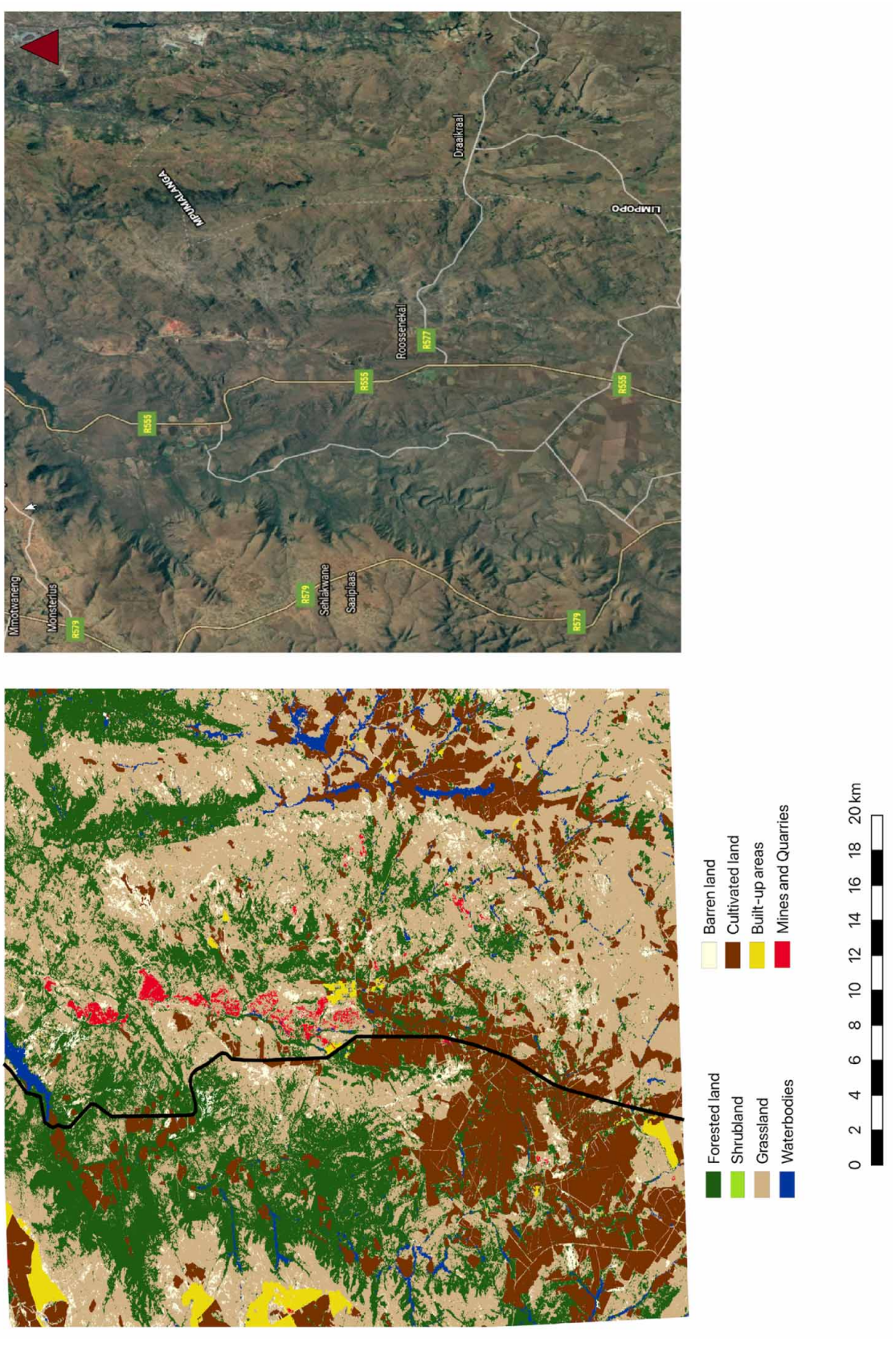

Figure 3. *Land usage map* ***(left)*** *compiled from Department of Environmental Affairs (2016) data, and map* ***(right)*** *of the area of interest retrieved from Google Earth (2018).*

validation data (normally generated from ground observations and measurements and or ancillary remote imagery), and the rows represent the data attained from the classification of the remotely sensed imagery. The error matrix not only depicts the map accuracy but the error as well (Congalton, 2001; Congalton and Green, 2002). Commission errors (Type II error) occur when pixels or sampling units are included in a category that it does not belong to, and omission errors (Type I error) are the exclusion of pixels or sampling units from the correct category (Congalton and Green, 2002). In addition to clearly depicting the errors of commission and omission and overall accuracy, the error matrix shows both the producer's accuracy (the accuracy of the map from the map maker's point of view) and the user's accuracy (the accuracy of the map from the user's point of view) (Story and Congalton, 1986).

To authenticate the landcover classification performance on the PlanetScope Analytic Ortho Tile, the classification algorithms were assessed using visual observations (using a reference map) and quantitative classification accuracy indicators. The overall classification algorithm accuracy, producer's accuracy, user's accuracy, and Kappa statistics were calculated in ENVI (Exelis Visual Information Solutions, 2017) for quantitative classification performance analysis. The Kappa statistic is a discrete multivariate technique (similar in function as the Chi-square analysis), used to evaluate the accuracy of a classification by comparing the level of agreement between the training data and the reference data (Cohen, 1960). The Kappa coefficient (attained from the Kappa statistic) is a value ranging from -1 to 1. A Kappa value 1 implies that there is a perfect agreement between the training and the reference or validation data and values less than 1 are indicative of less than perfect agreement (Cohen, 1960; Congalton and Green, 2002). See Cohen (1960); Congalton and Green (2002) for full formula sheet. Additionally, the significance of each classification algorithm was tested using the Z statistics denote by the formula found in Cohen (1960); Congalton and Green (2002).

The classification error matrices were further subjected to a pairwise comparison analysis, to determine if any two error matrices were significantly dissimilar from one another using the formula found in Cohen (1960); Congalton and Green (2002). The critical value is 1.96 at a 95% confidence level. Therefore, if the Z-value for error matrix is greater than 1.96 the error matrix or matrices are significantly better than a random classification or significantly dissimilar from each other, respectively (Congalton and Green, 2002).

Results

The *K-fold* cross-validation analysis yielded an R^2 value of 0.88 (an R^2 value close to 1 is an indicator a good match between the training and test data), an RMSE and an MAE of 5.57 and 4.56. Both the RMSE and MAE values do not have absolute good or bad thresholds and are dependent on the size of the data, but a general rule of thumb is that smaller values are better.

The training data was used in the classification of satellite imagery, using a common and an advanced algorithm, of the Eastern Limb of the Bushveld Complex and to detect and map magnetite. The test data was used to evaluate the performance of the classification. Tables 2 and 3 give a summary of the commission and omission errors and producers' and users' error for the Maximum Likelihood and Support Vector Machine classification algorithm. Figures 3 and 4 convey the landcover classification of the seven classes using the two different algorithms. Each is depicted in a different colour. Magnetite is depicted in navy blue in all the classification algorithms.

The Maximum Likelihood classification algorithm, the algorithm that had the highest accuracy (Table 2 and Figure 4), conveyed a clearer distinction between classes compared to the mixture of classes noted in Figure 4. Irrespective of the Maximum Likelihood classification algorithm illustrating better class categorization, a large proportion of the mining activity pixels were incorrectly classified as agricultural land (Table 2). However, this observation was not merely limited to the Maximum Likelihood classification algorithm, as similar observations were noted with the Support Vector Machine classification algorithm (Table 3). The commission errors for mining activities (Table 2 and 3) were higher in both

Table 2. Summary of commission and omission error and producer's and user's error for the Maximum Likelihood classification algorithm. The overall accuracy was 84.58%, the Kappa coefficient was 0.79 and the Z-value was 731.16.

Class	Commission (%)	Omission (%)	Producer's accuracy (%)	User's accuracy (%)
Agricultural land	18.09	6.65	93.35	81.91
Grassland and trees	6.13	3.8	96.2	93.87
Magnetite	11.34	23.59	76.41	88.66
Mining activities	54.54	91.98	8.02	45.46
Regolith	2.86	7.1	92.9	97.14
Residential areas	88.28	4.75	95.25	11.72
Waterbody	0	1.71	98.29	100

Table 3. Summary of commission and omission error and producer's and user's error for the Support Vector Machine learning algorithm. The overall accuracy was 80.89%, the Kappa coefficient was 0.73 and the Z-value was 606.60.

Class	Commission (%)	Omission (%)	Producer's accuracy (%)	User's accuracy (%)
Agricultural land	12.51	2.8	97.2	75.49
Grassland and trees	12.08	0	100	87.92
Magnetite	31.09	83.88	16.12	68.91
Mining activities	98.99	99.66	0.34	1.01
Regolith	8.84	21.61	78.39	91.16
Residential areas	0	27.79	72.21	100
Waterbody	0	1.33	98.67	100

classification algorithms, indicating misclassifications for the class. This is an indication of the similarity in the spectral reflectance of mining activities and agricultural land. Agricultural land, water bodies, and grassland and trees were seldom misclassified in the thematic maps. Statistical analyses revealed that the two classification algorithms performed better than a random classification, with each classification attaining a Z-value significantly higher than 1.96 at a 95% confidence level.

A pairwise comparison between the two algorithms revealed that the Maximum Likelihood classification algorithm was significantly different to the Support Vector Machine classification algorithm. The Maximum Likelihood classification

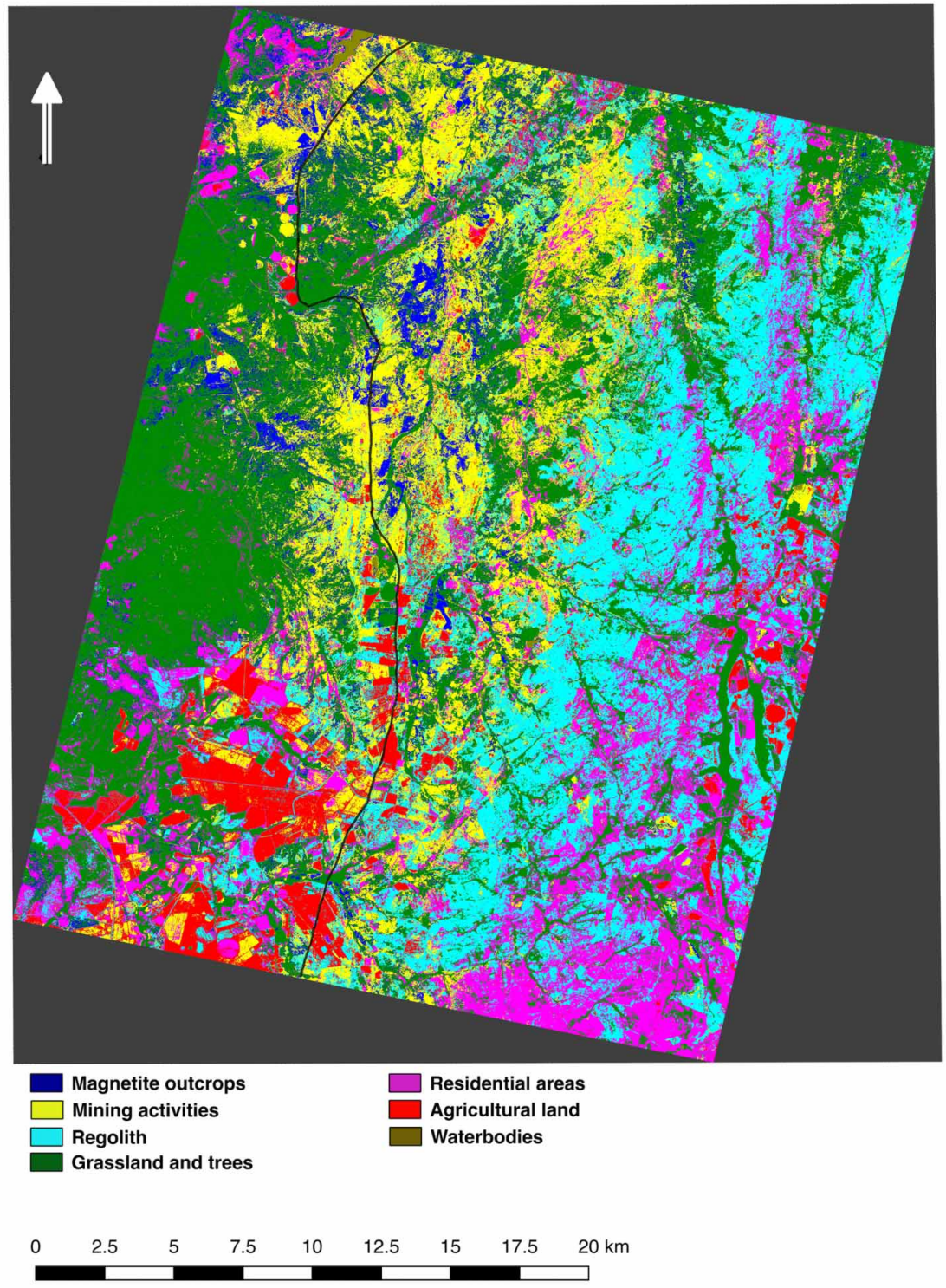

Figure 4. *Classification of study site using Maximum Likelihood classification algorithm. Different colours indicate different land class features. Magnetite is shown in navy blue.*

trees, as is evident from Table 3 and Figure 5. The main difference between the Maximum Likelihood (Figure 4) and Support Vector Machine (Figure 5) classification landcover map is the large proportion of the landscape that is classified as regolith and mining activities, which almost completely envelops areas that are agricultural land, grassland and trees, and residential areas, in the Support Vector Machine classification. Subsequently, the Support Vector classification algorithm has more errors of commission and errors of omission than the Maximum Likelihood classification algorithm, evident from Table 3.

Discussion

Although multispectral and hyperspectral imagery are two widely used components of remote sensing for lithological discrimination and classification, obtaining appropriate hyperspectral imagery for mineral and geological mapping is difficult because of the high costs and complexity of the treatment associated with hyperspectral remote sensing (Ge et al., 2018). However, the combination of high spatial multispectral remote sensing data (such as PlanetScope) with reliable textural and reference data is very effective in achieving good results.

This study aims at mapping magnetite potential areas using common and advanced classification algorithms on the Upper Zone of the Eastern Limb of the Bushveld Complex and to compare and contrast the performance of a common classification algorithm (Maximum Likelihood) over an advanced classification algorithms (Support Vector Machine). Of the two classification algorithms outputs evaluated in this study, the Maximum Likelihood classification algorithm performed best in the overall prediction accuracy of all seven classes (with an overall accuracy of 84.58%) and was the algorithm most fit for the detection and mapping of magnetite (with a producer's accuracy of 76.41% and a user's accuracy of 88.66%) in the Eastern Limb of the Bushveld Complex. The result was not in accordance to the expectations of the study, and additionally this result was in contrast to other studies that had compared the performance of common and advance classification algorithms (Pal and Mather, 2005; Joevivek and Chandrasekar, 2010; Otukei and Blaschke, 2010; Yu et al., 2012; Omeer et al., 2018). Szuster et al (2011), found the Support Vector Machine classification algorithm to be the best classification algorithm for separating man-made infrastructures from those of nature, irrespective of the similarity in spectral signatures.

Though the Support Vector Machine did not yield acceptably accurate results for the detection of magnetite, its overall accuracies were unexpectedly high. There are two plausible factors that may have accounted for the high overall accuracy levels in Support Vector Machines classification algorithm in this study. First, and the most noteworthy, is the prevalence of extensive and easily differentiable classes (e.g. grassland trees, agricultural area, and waterbodies), which indubitably contributed to the consistently high overall accuracies (see Table S1 and S2.) (Supplementary data files are archived in the South African Journal of Geology repository (https://doi.org/10.25131/sajg.123.0041.sup-mat)). The spatial limitation of the other classes relative to the aforementioned classes with a greater spatial capacity (i.e. grassland and trees, agricultural areas, and waterbodies) contributed to a high overall performance values or scores by curbing both the amount and spectral diversity of the pixels belonging to the spatially constrained classes (e.g. mining areas, residential areas and magnetite). The later mentioned factor likely led to the overfitting of certain other classes noted in Figure 4. Lastly, single developed classes were used in this study, which encompassed some landcover pixels being categorized as residential areas, despite including roads and other non-residential buildings.

The Maximum Likelihood and the Support Vector Machine classification algorithms both attained a Kappa value above 70%, with an overall accuracy of over 80%, which is a result akin to that found by studies conducted by He et al. (2015); Karan and Samadder (2016); Moeletsi and Tesfamichael (2018); Mondal et al. (2020). However, it must be noted that the overall accuracy of the Support Vector Machine classification algorithm was relatively high due to the fact that the majority of non-geological classes with the highest number of pixels were the pixels that had the highest accuracies (e.g. agricultural land, water bodies, regolith, and grassland trees). Since the overall accuracy formula is based on the number of pixels of each class, classes with a high pixel count are likely to positively skew the overall accuracy. In fact, with the high pixel count classes removed, the Support Vector Machine classification algorithm merely had a meagre 20.95% overall accuracy. In comparison, with the removal of the non-geological classes, the Maximum Likelihood classification algorithm attained an overall accuracy of 64.35%.

Despite prior successes of the Support Vector classification algorithm in lithological mapping, the Support Vector classification algorithm was not able to accurately detect exposed magnetite bodies. This may have been in part due to the spectral resolution of the imagery, the heterogeneity of the chemical mineralogical composition of the mining areas at the sub-pixel level, and algorithm high bias (when algorithms are underfitted, i.e. not having enough features for the target outputs). However, high bias algorithms do not benefit from more training data, but, they may benefit from more features or training data. The heterogeneity of chemical composition may have affected the resultant spectral purity of magnetite through the intimate or non-linear spectral combination of the spectra of end-members (Gupta, 2017). Other mineral or oxides (such hematite and limonite) found in association with weathered magnetite in magnetite bodies, may have contaminated the spectral response of magnetite causing it be correlated with the absorption bands of hematite and limonite.

As previously found by Hunt (1971), the increase in the size of magnetite grains equates to an increase in the reflectance of incident photons of light and absorption features. The different spectral signature of magnetite, owing to an increase in spectral reflectance may have led to some magnetite bodies being misclassified. Regardless of the rigorous pre-processing, the above-mentioned factors could have very well affected the spectral responses of the magnetite bodies. The aforementioned shortcomings are a result of using a sensor with four bands,

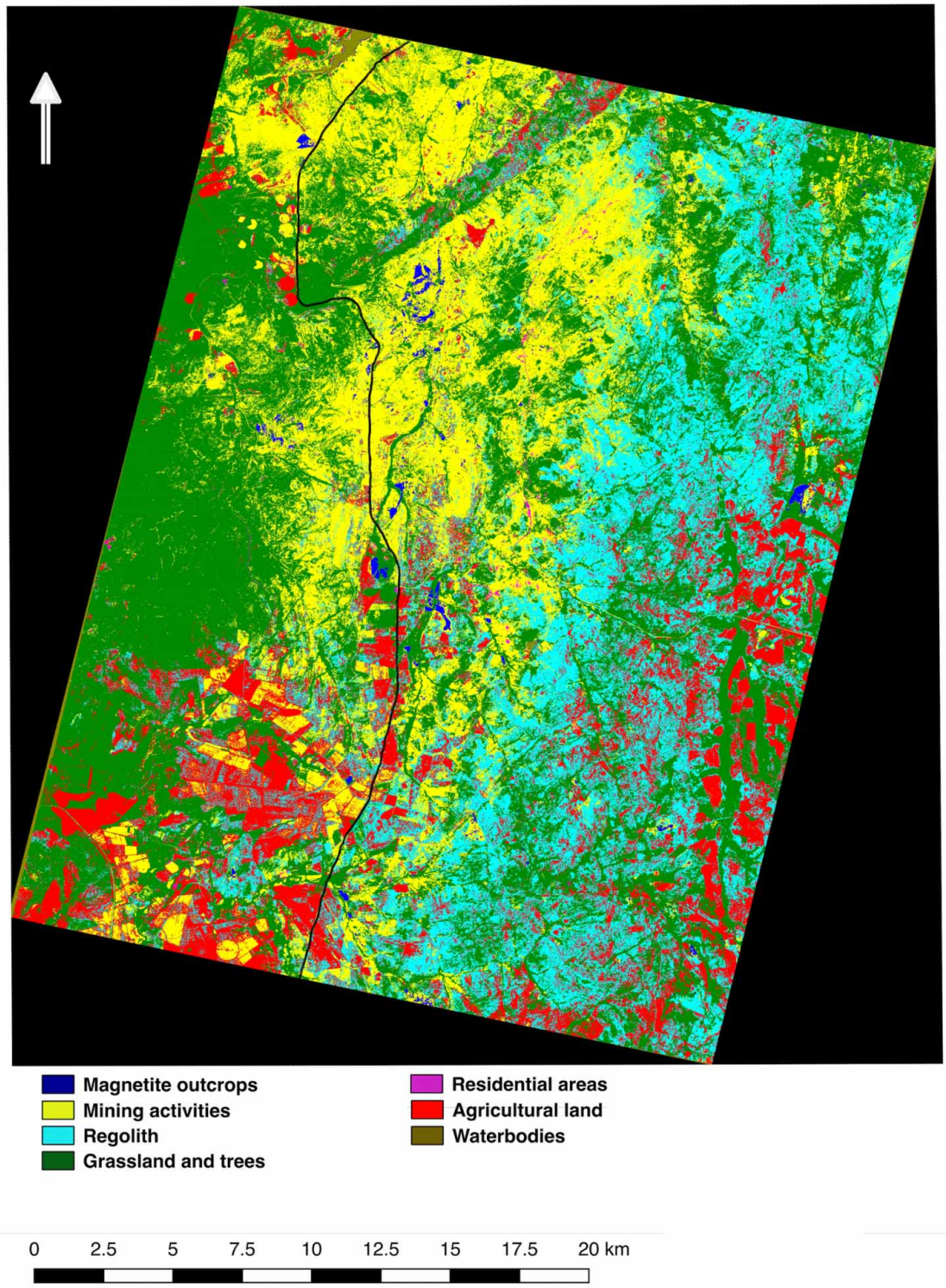

Figure 5. *Classification of study site using Support Vector Machine learning algorithm. Different colours indicate different land class features. Magnetite is shown in navy blue.*

algorithm producer's accuracy was higher than the Support Vector Machine classification algorithm for magnetite, with a prediction percentage of 76.41. The Support Vector Machine classification algorithm had a prediction percentage of 16.12. Additionally, the Maximum Likelihood classification algorithm was able to accurately distinguish magnetite 88.66% of the time, whereas the Support Vector Machine classification algorithm could do so 68.91% of the time.

The Support Vector classification algorithm was accurate in classifying most waterbodies, residential areas, and grassland and

which has broad wavelength ranges and therefore makes it difficult to distinguish the finer absorption characteristics of magnetite bodies. However, this was due to the trade-offs between spatial, spectral, and radiometric resolution of the sensor that was chosen and was a better fit for this undertaking. Hence, a sensor with a high or finer spectral resolution is essential when absorption lines of various geological features are located in the same spectral range with other geological features that interfere with each other. Using sensors with finer spectral resolutions (sensors with narrower band widths) thus creates the opportunity to identify some materials by their absorption-band characteristics (i.e. accurately discriminate some of the features that make up the remote sensing signal) and attenuate the interference.

The overall high accuracy classification of the Maximum Likelihood classification algorithm in this study suggests the classification algorithm may be advantageous in the detection and mapping of exposed magnetite bodies and that remote sensing methods are effective tools for geological mapping and mineral exploration, especially in iron oxides (despite the other geological features obscuring the spectral reflectance of the focal substrate). Indeed, full knowledge of the performance differences of each classification algorithm is crucial for the choice of a classification algorithm for a particular scene and application. As with many remote sensing applications, the greater onus should be placed on the precision and accuracy of the dataset than the classification algorithms used for analysis. While the choice of classification algorithm will undoubtedly influence the success of mineral detection and mapping, the accessibility, quality, and processing of geology data will have an even greater stronger influence and impact on the results. This includes the size of the study area and the spatial and spectral resolution of the data. In essence, the choice of the most appropriate algorithm should be based on the characteristics of the data, as well as, the research objectives.

Conclusion

The present study focused on the remote sensing capability and Maximum Likelihood and Support Vector Machine classification algorithms in mapping the occurrence of magnetite in the Eastern Limb of the Bushveld Complex. This study revealed that the occurrence of magnetite could be successfully detected using the common traditional classification algorithms such as the Maximum Likelihood classifier. The results attained from the Maximum Likelihood classification algorithm indicated that the producer's and a user's accuracies were 76.41% and 88.66%, respectively. The computed kappa coefficient was 0.79, illustrating a high categorical and overall accuracy. The thematic map derived from the Maximum Likelihood classification algorithm had an overall accuracy of 84.58%. Overall, this study suggests the relevance and efficiency of using the common traditional classification algorithm – Maximum Likelihood over the advanced classification algorithms – Support Vector Machine, especially for studies with relatively small datasets. And despite the accuracy of common traditional classification algorithms and advanced classification algorithms, it is worth noting that remote sensing should not solely be used as decision-making tools or replacements for direct fieldwork but should be amalgamated with different datasets and the knowledge of a specialist.

References

Abrams, M.J., Brown, D., Lepley, L. and Sadowski, R., 1983. Remote sensing for porphyry copper deposits in southern Arizona. Economic Geology 78, 591-604.

Agar, B. and Coulter, D., 2007. Remote sensing for mineral exploration - a decade perspective 1997-2007. In Proceedings of Exploration 7, 109-136.

An, P., Chung, C.J.F. and Rencz, A.N., 1994. A preliminary study of alteration mapping from airborne geophysical and remote sensing data using feed-forward neural networks. In SEG Technical Program expanded Abstracts 1994, 837-840.

Babakan, S. and Oskouei, M.M., 2014. Integrated use of multispectral remote sensing and GIS for primary gold favorability mapping in Lahroud Region (NW Iran). Journal of Tethys 2, 228-241.

Campbell, J.B. and Wynne, R.H., 2011. Introduction to remote sensing, vol. 5, Guilford Press, New York, 67-87.

Cawthorn, R., 1994. Growth nodes at the base of magnetitite layers in the Upper Zone of the Bushveld Complex. South African Journal of Geology 97, 455-461.

Chien, Y., 1974. Pattern classification and scene analysis. IEEE Transactions on Automatic Control 19, 462-463.

Chistyakova, S., Latypov, R. and Youlton, K., 2019. Multiple Merensky Reef of the Bushveld Complex, South Africa. Contributions to Mineralogy and Petrology 174, 3-26.

Clark, R.N. and Roush, T.L., 1984. Reflectance spectroscopy: Quantitative analysis techniques for remote sensing applications. Journal of Geophysical Research: Solid Earth 89, 6329-6340.

Cloutis, E.A., 1996. Review article hyperspectral geological remote sensing: evaluation of analytical techniques. International Journal of Remote Sensing 17, 2215-2242.

Cohen, J., 1960. A coefficient of agreement for nominal scales. Educational and psychological measurement 20, 37-46.

Congalton, R.G., 2001. Accuracy assessment and validation of remotely sensed and other spatial information. International Journal of Wildland Fire 10, 321-328.

Congalton, R.G., and Green, K., 2002. Assessing the accuracy of remotely sensed data: principles and practices, vol. 2, CRC Press, New York, 55-62.

Congalton, R.G., Oderwald, R.G. and Mead, R.A., 1983. Assessing Landsat classification accuracy using discrete multivariate analysis statistical techniques. Photogrammetric engineering and remote sensing 49, 1671-1678.

Continuum Analytics., 2019. Anaconda Python (Version Python 3.7 version). Retrieved from https://www.anaconda.com/distribution/

Department of Environmental Affairs., 2016. GIS Data Downloads. Available: https://egis.environment.gov.za/gis_data_downloads [Accessed 10 February 2020].

Drury, S.A., 2001. Image interpretation in geology, vol. 3, Chapman & Hall, Cheltenham, 35-65.

Eales, H.V. and Cawthorn, R.G., 1996. The Bushveld Complex. Development in Petrology. Elsevier 51, 181-229.

ERDAS., 2005. ERDAS field guide. Copyright Leica Geosystems Geospatial Imaging, LLC.

Exelis Visual Information Solutions., 2017. Environment for visualizing images. In: Exelis Visual Information Solutions

Fatima, K., Khattak, U.K. and Kausar, A.B., 2013. Selection of appropriate classification technique for lithological mapping of Gali Jagir area, Pakistan. International Journal of Earth Sciences and Engineering 7, 964-971.

Fischer, L.A., Wang, M., Charlier, B., Namur, O., Roberts, R.J., Veksler, I.V. and Holtz, F., 2016. Immiscible iron-and silica-rich liquids in the Upper Zone of the Bushveld Complex. Earth and Planetary Science Letters 443, 108-117.

Foody, G.M., 2008. Harshness in image classification accuracy assessment. International Journal of Remote Sensing 29, 3137-3158.

Foody, G.M., Campbell, N.A., Trodd, N.M. and Wood, T.F., 1992. Derivation and applications of probabilistic measures of class membership from the maximum-likelihood classification. Photogrammetric engineering and remote sensing 58, 1335-1341.

Fox, J. and Weisberg, S., 2011. An R Companion to Applied Regression. Using car Functions in Other Functions, vol.2, Sage, California, 385-420.

Ge, W., Cheng, Q., Tang, Y., Jing, L. and Gao, C., 2018. Lithological classification using sentinel-2A data in the Shibanjing ophiolite complex in inner Mongolia, China. Remote Sensing 10, 638.

Google Earth (Cartographer)., 2018. Roossenekal -25.193722, 29.924991, elevation 2253.996m. 3D map. Available: https://www.google.com/maps/place/Roossenekal/data=!4m2!3m1!1s0x1ec1e58802a9a6dd:0x48d693c133d31ee9?sa=X&ved=2ahUKEwiqmqegjeLjAhXWSxUIHT8xACUQ8gEwD3oECAsQBA [Accessed 1 December 2019].

Grant , R.C., 2015. The Bushveld Complex, South Africa. In: B. Charlier (Editor), Layered Intrusions, vol. 1, Springer Science, Dordrecht, 517-587.

Gupta, R.P., 2017. Remote sensing geology, vol. 3, Springer-Verlag, Berlin, 23-34.

Harne, D. M. and Von Gruenewaldt, G., 1995. Ore-forming processes in the upper part of the Bushveld complex, South Africa. Journal of African Earth Sciences 20, 77-89.

He, J., Harris, J.R., Sawada, M. and Behnia, P., 2015. A comparison of classification algorithms using Landsat-7 and Landsat-8 data for mapping lithology in Canada's Arctic. International Journal of Remote Sensing 36, 2252-2276.

Hunt, G. R., 1971. Visible and near-infrared spectra of minerals and rocks: III. Oxides and hydro-oxides. Modern Geology 2, 195-205.

Izawa, M.R., Cloutis, E.A., Rhind, T., Mertzman, S.A., Applin, D.M., Stromberg, J.M. and Sherman, D.M., 2019. Spectral reflectance properties of magnetites: Implications for remote sensing. Icarus 319, 525-539.

James, G., Witten, D., Hastie, T. and Tibshirani, R., 2014. An Introduction to Statistical

Learning: With Applications in R, vol.112, Springer Publishing Company, Incorporated, New York, 18.

Jensen, J.R., 2005. Introductory digital image processing: a remote sensing perspective, vol. 2, Prentice Hall, New Jersey, 330-344.

Jia, K., Wu, B., Tian, Y., Zeng, Y. and Li, Q., 2011. Vegetation classification method with biochemical composition estimated from remote sensing data. International Journal of Remote Sensing 32, 9307-9325.

Joevivek, V. and Chandrasekar, N., 2010. Comparison of Supervised Classification Methods for Efficiently Locating Possible Mineral Deposits using Multispectral Remote Sensing data. International Journal of Advanced Research in Computer Science 1, 3.

Joseph, A. and Bamidele, O., 2018. Application of remote sensing method for geological interpretation of Sokoto Plain, Nigeria. South African Journal of Geomatics 7, 360-371.

Karan, S.K. and Samadder, S.R., 2016. Accuracy of land use change detection using support vector machine and maximum likelihood techniques for open-cast coal mining area. Environmental monitoring and assessment 188, 486.

Kavzoglu, T. and Colkesen, I., 2009. A kernel functions analysis for support vector machines for land cover classification. International Journal of Applied Earth Observation and Geoinformation 11, 352-359.

Kavzoglu, T. and Reis, S., 2008. Performance analysis of maximum likelihood and artificial neural network classifiers for training sets with mixed pixels. GIScience & Remote Sensing 45, 330-342.

Kemp, J.N., Zietsman, H.L. and Stevens, G., 2005. Evaluating image classification techniques on Aster data for lithological discrimination in the Barberton Greenstone Belt, Mpumalanga, South Africa. M.Sc thesis, University of Stellenbosch, Stellenbosch, 1-2.

Li, J.Q., Yi, H., Ren, G.L., Gao, T., Yang, M., Han, H.H. and Yang, J.L., 2016. High resolution remote sensing and potential analysis of iron ore prospecting–Taking Datong Township, West KunLun Area for example. IOP Conference Series: Earth and Environmental Science 46, 1-6.

Maila, R.P., 2015. Geochemistry of magnetite layers in the upper zone of the Bushveld Complex, South Africa. M.Sc, WITS University, South Africa, 31-35.

Manuel, R., Brito, M., Chichorro, M. and Rosa, C. 2017. Remote sensing for mineral exploration in central Portugal. Minerals 7, 184.

Mather, P. and Tso, B., 2016. Classification methods for remotely sensed data, vol. 2, CRC press, Boca Raton, 54-102.

Mather, P.M. and Koch, M., 2011. Computer processing of remotely-sensed images: an introduction, vol. 4, John Wiley & Sons, New Jersey, 271-299.

McCarthy, T., Cawthorn, R.G., Wright, C. and McIver, J., 1985. Mineral layering in the Bushveld Complex; implications of Cr abundances in magnetite from closely spaced magnetitite and intervening silicate-rich layers. Economic Geology 80, 1062-1074.

Metternicht, G. and Zinck, J., 2003. Remote sensing of soil salinity: potentials and constraints. Remote Sensing of Environment 85, 1-20.

Moeletsi, R.S. and Tesfamichael, S.G., 2018. Comparison of Landsat and ASTER in Land Cover Change Detection within Granite Quarries. In GISTAM, 187-195.

Mondal, A., Kundu, S., Chandniha, S.K., Shukla, R. and Mishra, P., 2012. Comparison of support vector machine and maximum likelihood classification technique using satellite imagery. International Journal of Remote Sensing and GIS 1, 116-123.

Ngcofe, L. and Van Niekerk, A., 2016. Advances in optical earth observation for geological mapping: A Review. South African Journal of Geomatics 5, 1-16.

Omeer, A.A., Deshmukh, R.R., Gupta, R.S. and Kayte, J.N., 2018. Land Use and Cover Mapping Using SVM and MLC Classifiers: A Case Study of Aurangabad City, Maharashtra, India. International Conference on Recent Trends in Image Processing and Pattern Recognition. Springer, Singapore, 482-492

Otukei, J.R. and Blaschke, T., 2010. Land cover change assessment using decision trees, support vector machines and maximum likelihood classification algorithms. International Journal of Applied Earth Observation and Geoinformation 12, S27-S31.

Pal, M. and Mather, P., 2005. Support vector machines for classification in remote sensing. International Journal of Remote Sensing 26, 1007-1011.

Planet Team (Cartographer)., 2018. Planet Application Program Interface: In Space for Life on Earth. Retrieved from https://api.planet.com

QGIS Development Team., 2015. QGIS Geographic Information System. Open Source Geospatial Foundation Project. URL: http://qgis. osgeo. org.

R Core Team., 2016. R: A language and environment for statistical computing. R Foundation for Statistical Computing, Vienna.

Rajendran, S., Thirunavukkaraasu, A., Poovalingaganesh, B., Kumar, K.V. and Bhaskaran, G., 2007. Discrimination of low-grade magnetite ores using remote sensing techniques. Journal of the Indian Society of Remote Sensing 35, 153.

Reynolds, I.M., 1985. Contrasted mineralogy and textural relationships in the uppermost titaniferous magnetite layers of the Bushveld Complex in the Bierkraal area north of Rustenburg. Economic Geology 80, 1027-1048.

Roelofse, F. and Ashwal, L.D., 2012. The Lower Main Zone in the Northern Limb of the Bushveld Complex- a >1.3 km Thick Sequence of Intruded and Variably Contaminated Crystal Mushes. Journal of Petrology 53, 1449-1476.

Rowan, L.C., Mars, J.C. and Simpson, C.J., 2005. Lithologic mapping of the Mordor, NT, Australia ultramafic complex by using the Advanced Spaceborne Thermal Emission and Reflection Radiometer (ASTER). Remote Sensing of Environment 99, 105-126.

SACS., 1980. Stratigraphy of South Africa, vol. 1. R & E Publishers, Pretoria, 376, 381.

Shirazi, A., Hezarkhani, A., Shirazy, A. and Shahrood, I., 2018. Remote Sensing Studies for Mapping of Iron Oxide Regions, South of Kerman, IRAN. International Journal of Science and Engineering Applications 4, 45-51.

Story, M. and Congalton, R.G., 1986. Accuracy assessment: a user's perspective. Photogrammetric engineering and remote sensing 52, 397-399.

Szuster, B.W., Chen, Q. and Borger, M., 2011. A comparison of classification techniques to support land cover and land use analysis in tropical coastal zones. Applied Geography 31, 525-532.

Tegner, C., Cawthorn, R.G. and Kruger, F.J., 2006. Cyclicity in the Main and Upper Zones of the Bushveld Complex, South Africa: crystallization from a zoned magma sheet. Journal of Petrology 47, 2257-2279.

Vapnik, V., 1999. An Overview of Statistical Learning Theory, vol. 5. IEEE Transactions on Neural Networks, New York, 988-999.

Vapnik, V., 2013. The nature of statistical learning theory, vol. 1. Springer Science & Business Media, New York, 133-155.

Von Gruenewaldt, G., 1971. A petrographical and mineralogical investigation of the rocks of the Bushveld Igneous Complex in the Tauteshoogte-Roossenekal area of the Eastern Transvaal. Doctoral dissertation, University of Pretoria, 154-157.

Von Gruenewaldt, G., 1976. Sulfides in the upper zone of the eastern Bushveld Complex. Economic Geology 71, 1324-1336.

Wang, L., and Qu, J.J., 2009. Satellite remote sensing applications for surface soil moisture monitoring: A review. Frontiers of Earth Science in China 3, 237-247.

Wickham, H., Francois, R., Henry, L. and Müller, K., 2015. dplyr: A Grammar of Data Manipulation. R package version 0.4. 3. R Found. Stat. Comput., Vienna. https://CRAN. R-project. org/package= dplyr.

Wickham, H., Hester, J., Francois, R., Jylänki, J. and Jørgensen, M., 2017. readr: read rectangular text data. R package version 1.1. 1. R Foundation for Statistical Computing.

Wickham, H. and Henry, L., 2018. tidyr: easily tidy data with 'spread()' and 'gather() Functions. R package version 0.8.1. https://CRAN.R-project.org/package=tidyr.

Willemse, J., 1969. The geology of the Bushveld Igneous Complex, the largest repository of magmatic ore deposits in the world. Paper presented at the Magmatic Ore Deposits. a Symposium.

Yu, L., Porwal, A., Holden, E.J. and Dentith, M.C., 2012. Towards automatic lithological classification from remote sensing data using support vector machines. Computers & Geosciences 45, 229-239.

Editorial handling: M.A. Elburg.